Solid-State Electronics 209 (2023) 108756

Contents lists available at ScienceDirect

Solid State Electronics

journal homepage: www.elsevier.com/locate/sse

# Ultrathin four-quadrant silicon photodiodes for beam position and monitor applications: Characterization and radiation effects

J.M. Rafí [a,*], D. Quirion [a], M. Duch [a], I. Lopez Paz [a], V. Dauderys [a], T. Claus [a], N. Moffat [a], B. Molas [b], I. Tsunoda [c], M. Yoneoka [c], K. Takakura [c], G. Kramberger [d], M. Moll [e], G. Pellegrini [a]

[a] Instituto de Microelectrónica de Barcelona, CNM-CSIC, Campus UAB, 08193 Bellaterra, Spain
[b] ALBA Synchrotron, Carrer de la Llum 2-26, 08290 Cerdanyola del Vallès, Barcelona, Spain
[c] National Institute of Technology (KOSEN), Kumamoto College, 2659-2 Suya, Kumamoto, Japan
[d] Jozef Stefan Institute, SI-1000 Ljubljana, Slovenia
[e] European Organization for Nuclear Research (CERN), 1211 Geneva, Switzerland

ARTICLE INFO

The review of this paper was arranged by Prof. Sorin Cristoloveanu

*Keywords:*
Ultrathin silicon beam position monitors
Four quadrant photodiodes
Radiation effects
Interquadrant resistance
X-ray synchrotron
Pulsed laser beam transient current technique

ABSTRACT

Ultrathin semiconductor photodiodes are of interest for beam position and monitoring in X-ray synchrotron beamlines and particle therapy medical applications. In this work, single and four-quadrant diodes have been fabricated on ultrathin Si films with thicknesses of 10 μm, 5 μm and 3 μm from silicon on insulator (SOI) substrates. Physical and electrical characterization of the devices has been carried out. Good functional electrical characteristics have been obtained for the devices fabricated on the different silicon thicknesses. The impact of electron, neutron and proton irradiations on the electrical characteristics has been studied for the 10 μm-thick devices. In spite of the observed diode leakage current increase and positive charge trapping in interquadrant isolation oxide, functional operation as radiation detector is verified upon illumination with a pulsed laser beam transient current technique.

## 1. Introduction

Single and four-quadrant (4Q) semiconductor photodiodes are very common beam intensity and position diagnostic devices for hard X-ray synchrotron beamlines (Fig. 1) [1], and they are also of interest for real time monitoring and dosimetry in particle therapy medical applications [2]. X-ray beam position monitors (XBPMs), are to be thinner than 10 μm when made of silicon to achieve X-ray transmission higher than 90% for photon energies above 10 keV [3]. The need of installing several devices along the beam path has pushed towards the use of diamond due to lower absorption of carbon with respect to Si [4]. Owing to their lower dark current, lower susceptibility to temperature and visible light conditions, and potential radiation hardness, there is also interest in silicon carbide (SiC) for some of these applications [5–7]. However, ultrathin Si devices are still advantageous in terms of cost and sensing area and some first types of ultrathin (down to 10 μm or 5 μm) photodiodes have been studied [1,3,8].

As a progress to previous works, here ultrathin single and 4Q diodes with silicon thicknesses down to 3 μm have been successfully fabricated using silicon on insulator (SOI) substrates. Physical and electrical characterization of the devices is carried out and the impact of different particle irradiations, as well as operation as radiation detector, is assessed for the 10 μm-thick devices.

## 2. Device fabrication

Single and 4Q diodes have been fabricated at IMB-CNM-CSIC cleanroom on ultrathin Si films with thickness of 10 μm, 5 μm and 3 μm from SOI substrates. The process for the 10 μm devices is based on a technology developed to fabricate large area thin detectors [9]. It involves direct wafer bonding between an oxidized and n+ implanted (final device back side ohmic contact) high resistivity (>3 kΩ·cm) FZ Si wafer and an oxidized handle wafer, top wafer thinning, p-on-n device processing, and back side deep anisotropic etching [8,9]. Four mask levels are used for the entire process (p+ implant, metallization, passivation and back side etch). A schematic cross section of a fabricated 10 μm-Si 4Q diode is shown in Fig. 2. In order to further improve transmission, the process was adapted for the fabrication of thinner

* Corresponding author.
*E-mail address:* jm.rafi@csic.es (J.M. Rafí).

https://doi.org/10.1016/j.sse.2023.108756

Available online 30 August 2023

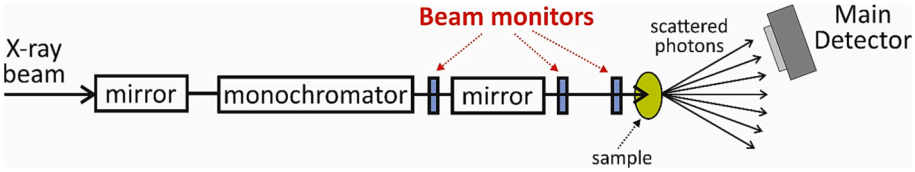


**Fig. 1.** Example of transmissive beam monitors setup in an X-ray beamline.

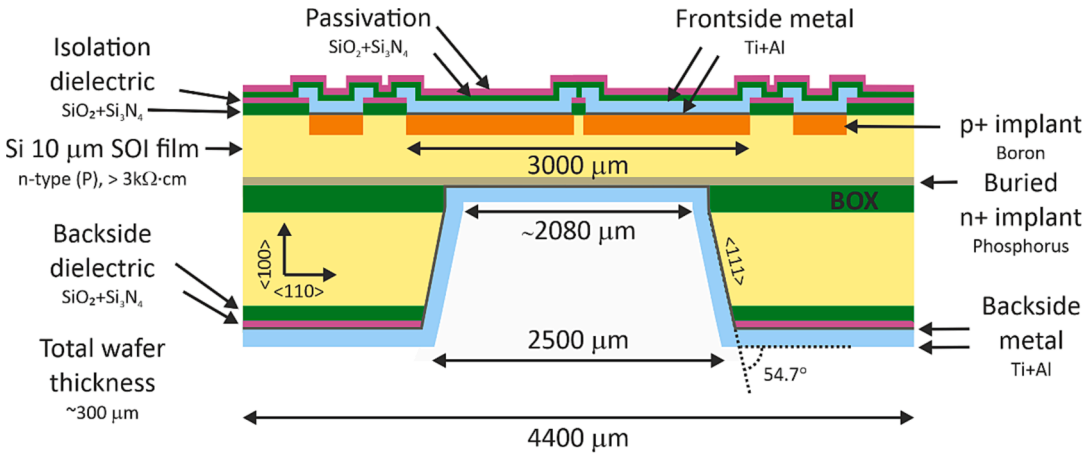


**Fig. 2.** (a) Schematic cross section (not drawn to scale) of a fully metallized 4Q diode with its guard ring fabricated on a 10 µm Si SOI layer.

devices on 5 µm SOI layers. To minimize reduction of active detector depth, shallower As implantation for the buried n+ implant and reduced thermal budget was implemented. This was further improved for the case of the 3 µm devices fabrication, where thinner metal layers of refractory metal (200 nm W instead of the 30 nm Ti plus 700 nm Al stack used for 10 µm and 5 µm devices) was used to allow back-end backside n+ implantation. Single as well as 4Q diodes implementing different metallization approaches, full or perimetric ring, to allow test with laser techniques, were included in the mask set.

## 3. Characterization and radiation effects

Fig. 3(a) shows a picture of a processed Si wafer with 5 µm-thick devices, where fully-metallized devices can be mainly observed in the upper half and right part of the wafer. Fig. 3(b) shows a front picture of a 4Q diode fabricated on a 3 µm-thick SOI silicon layer with contacting test probes. In this example device, interquadrant distance is 4 µm and the back side etched area can be distinguished in the picture as a central square-shaped region with different color tone. To maximize X-ray transmission, front metallization is only implemented here in peripherical 20 µm-wide regions corresponding to the outer borders of the quadrants. Different device cross section images, near the back etch corner and in the central interquadrant region are shown in Fig. 3(c) and 3(d), respectively, for a device fabricated on a 3 µm-thick SOI film. Membrane bending, due to metal-induced stress, was only observed for the case of the thinner devices (3 µm) with full metallization. Fig. 3(e) and 3(f) show 3D optical profiler results, with typical height profiles in the range of a few tens of microns over the 3 µm-thick devices.

Electrical characterization of the devices included both, current–voltage (I–V) and interquadrant resistance measurements ($R_{inter-quadrant}$) [8], to assess electrical isolation between the quadrants, and they showed good functional characteristics for the devices fabricated on the different silicon thicknesses. Fig. 4(a) shows measured I–V curves corresponding to one hundred 10 µm-thick Si p-n diodes from a single wafer map measurement, where good repeatability and low spreading is observed for current levels above the experimental resolution limit. The results were not so uniform for the case of the devices fabricated on the thinner layers, but good functional characteristics with reasonable yield were also achieved. In this way, Fig. 4(b) shows an example of I–V curves measured for p-n diodes fabricated on the different thicknesses, whereas Fig. 4(c) shows a wafer map for leakage current measured at a fixed reverse voltage of 3 V corresponding to 3 µm-thick devices. Interestingly, slightly higher leakage currents were generally obtained for the case of the fully metallized devices (Fig. 3(a)) exhibiting the membrane bending described in Fig. 3 results.

One important requirement in XBPMs is their radiation hardness and stability of the signal. This may be especially important in particle therapy medical applications. Although no displacement damage in the semiconductor crystalline lattice is expected under X-rays synchrotron applications, the high radiation doses may still be responsible for charge trapping and generation of radiation-induced interface traps in the dielectric layers used in their isolation and passivation [7]. In order to investigate radiation hardness of the devices, 2 MeV electron, neutron and 24 GeV/c proton irradiations were performed firstly on the 10 µm-thick devices at Takasaki-QST in Japan, JSI TRIGA in Slovenia, and CERN PS-IRRAD in Switzerland, respectively. The reported equivalent hardness factors for nonionizing energy loss (NIEL) in silicon with respect to 1 MeV neutrons are $2.49 \times 10^{-2}$, 0.9 and 0.56, respectively [7]. I–V characteristics measured for 10 µm-thick devices at different electron irradiation fluences are plotted in Fig. 5(a), where a progressive increase in leakage current with irradiation fluence can be seen. This is further observed in Fig. 5(b), where the leakage current measured at a

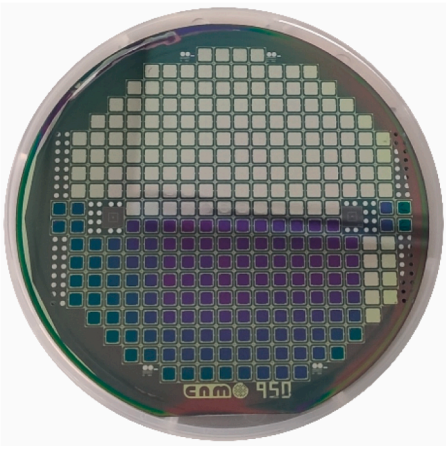


(a)

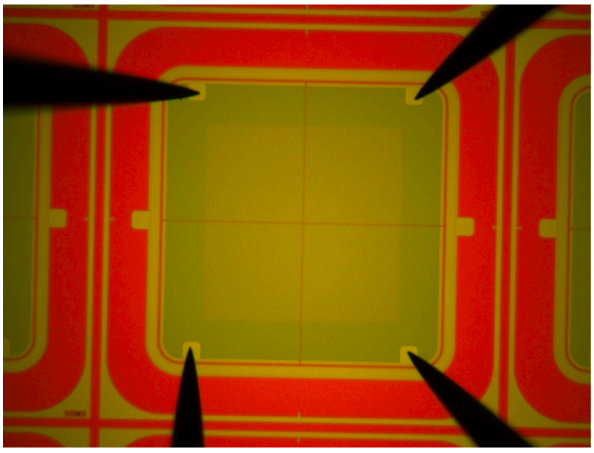

(b)

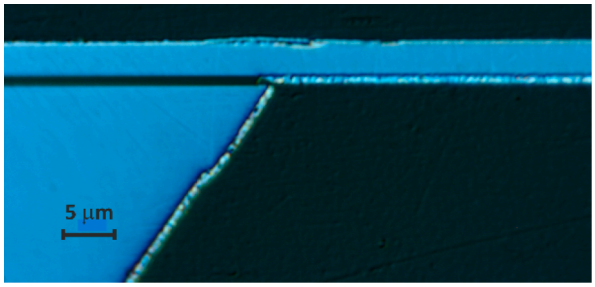


(c)

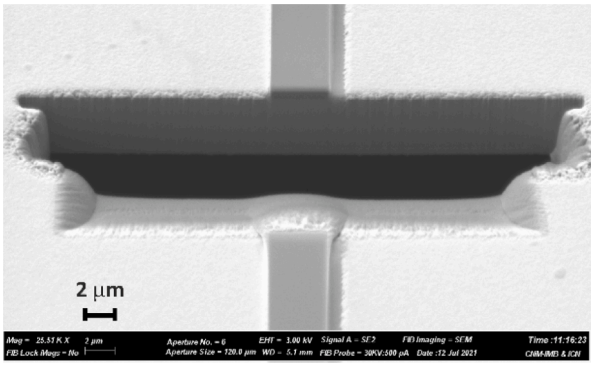


(d)

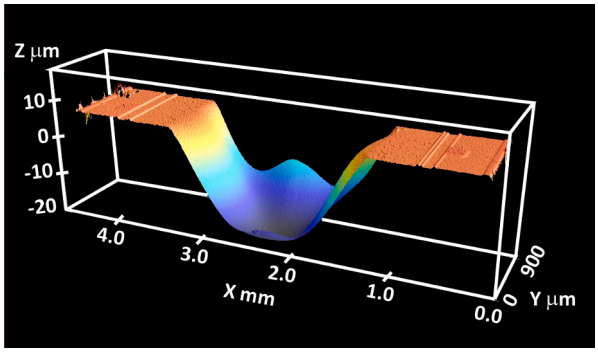


(e)

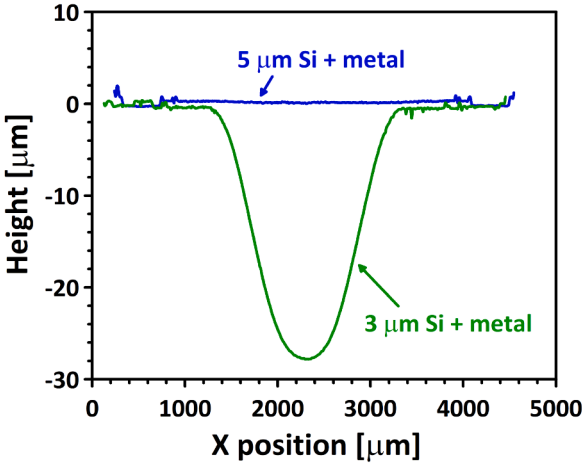


(f)

**Fig. 3.** (a) Front side picture of a processed Si wafer with 5 µm-thick devices. (b) Front picture of a 3 µm-thick 4Q diode with test probes. (c) Optical picture of mechanical cross section near back etch corner and (d) FIB-SEM cross section image of interquadrant region of a fabricated device on a 3 µm-thick SOI film. (e) 3D optical profiler measurement of surface height for a portion of a fully metallized 3 µm-thick Si device. (f) Measured height profiles for 5 µm-thick and 3 µm-thick devices with full metallization.

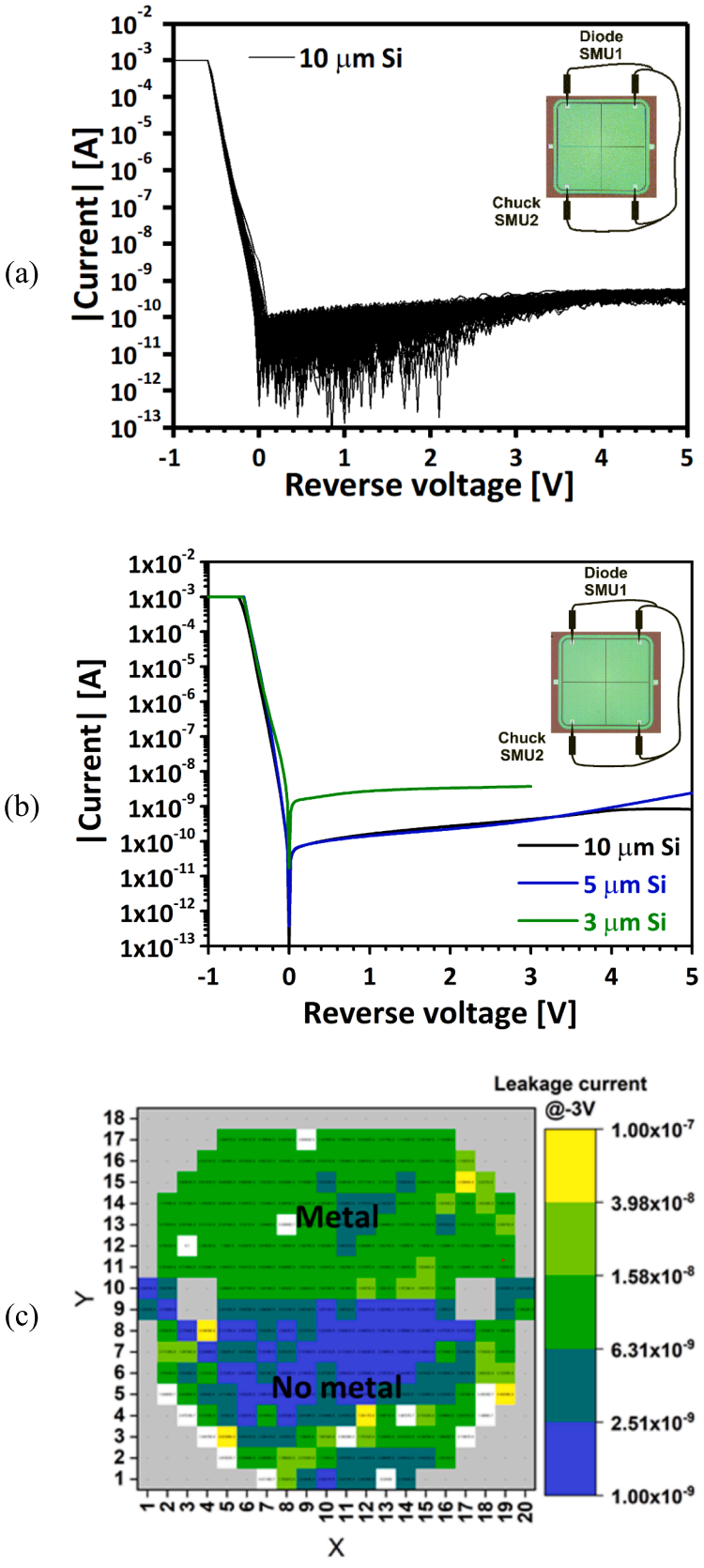


**Fig. 4.** (a) Measured I–V curves corresponding to one hundred 10 μm-thick Si p-n diodes from a single wafer map measurement. (b) Example I–V curves measured for p-n diodes fabricated on 10, 5 and 3 μm-thick Si layers. (c) 3 μm-thick wafer map results for diode leakage current at a fixed reverse voltage of 3 V. As indicated in (a) and (b) insets, I–V characterization was performed with all 4 quadrants shorted. Diode area is 0.09 $cm^2$.

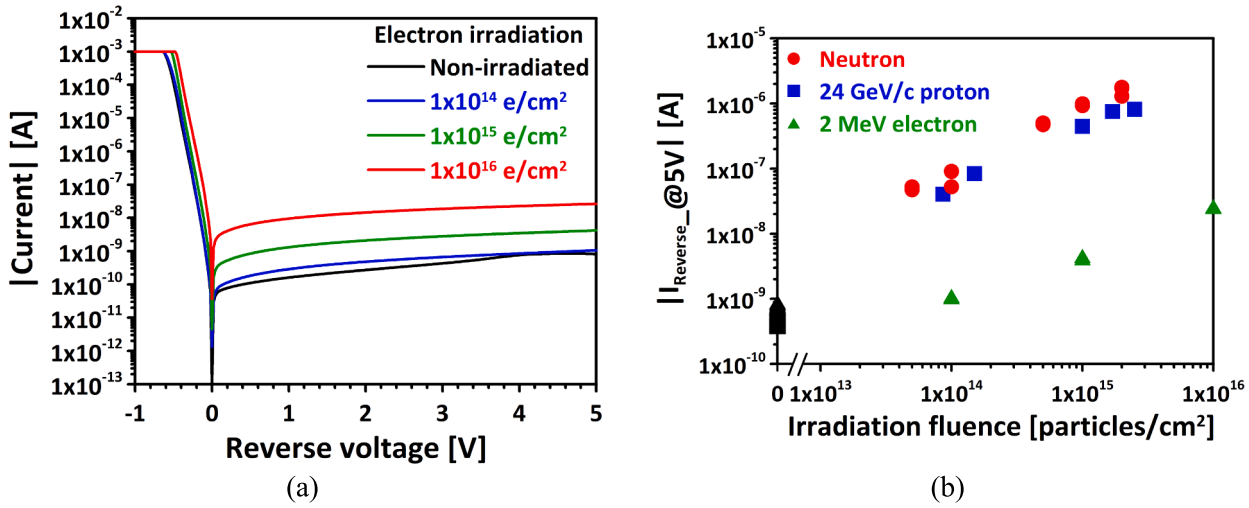


**Fig. 5.** (a) I–V characteristics measured for 10 μm-thick p-n diodes at different 2 MeV electron irradiation fluences. (b) Reverse current measured @ 5 V for 10 μm-thick p-n diodes at different electron, neutron and proton fluences. Diode area is 0.09 $cm^2$.

fixed reverse bias of 5 V has been plotted against irradiation fluence for different particle irradiations. The leakage current increase is attributed to radiation-induced defects actuating as generation-recombination centers. From the figure, values around $1.3 \times 10^{-17}$ A/cm and $0.6 \times 10^{-17}$ A/cm have been extracted for the leakage current damage rate (α) for neutrons and protons, respectively (with $I_{vol} = \alpha \cdot \phi$ and $I_{vol} \equiv I/(\text{area} \times \text{depletion depth})$), being these in the range of published results for irradiated bulk silicon detectors [7].

In order to evaluate possible radiation effects on diode interquadrant isolation, on wafer non back-etched MOS structures implementing the interquadrant isolation stack (520 nm $SiO_2$ + 185 nm $Si_3N_4$) as gate oxide were also studied. Fig. 6(a) shows measured C-V characteristics at different neutron irradiation fluences, indicating positive charge trapping in the dielectric. From the flat band voltage ($V_{fb}$) shifts of the measured C-V curves, an estimation of the oxide effective trapped charge density ($N_t$), defined as a fixed charge located at the silicon/dielectric interface, has been obtained [8]. It is based on the comparison of the extracted $V_{fb}$ values with the expected figures for an ideal MOS structure. The extracted values for $N_t$ are given in Fig. 6(b) for different electron, neutron and proton fluences. Positive charge trapped densities in the range of a few times $10^{12}$ $cm^{-2}$ are obtained after the highest fluences. For the purpose of investigating any possible impact of the observed radiation-induced charge trapping on electrical isolation between the quadrants, $R_{interquadrant}$ measurements were carried out. For these measurements, the current at one fixed quadrant ($Q_1$) is assessed as a function of a voltage sweep performed on the other three electrically shorted quadrants ($Q_2$, $Q_3$ and $Q_4$), while keeping a fixed functional substrate (chuck) voltage ($V_{back}$) [8]. A reduction of $R_{interquadrant}$ values with increasing irradiation fluences has been observed (Fig. 6(c)), however, electrical isolation between the quadrants is still preserved, as supported by the high $R_{interquadrant}$ values maintained.

Finally, the performance as radiation detectors of such ultrathin devices has innovatively been investigated by means of a scanning (with 10 μm steps) transient current technique [10], with a pulsed 10 μm-narrow violet (404 nm) laser beam, where the measured device signal response has been analyzed (Fig. 7(a)). 3D plots of collected charge and 2D contours of transient amplitudes measured for 2 adjacent quadrants of 10 μm-thick Si non-irradiated and a $5x10^{14}$ $n/cm^2$ irradiated devices are shown in Fig. 7(b-d). Note that in these devices with metallization limited to the outer borders of the quadrants the magnitude of pulse peak is greater near device periphery, while the total collected charge (integrated pulse) is more uniform for all the active device area. From Fig. 7, the detector remains operative after $5x10^{14}$ neutron/$cm^2$, although reductions in the range of 20 percent and 10 percent are observed for the magnitude of pulse peak and collected charge, respectively.

## 4. Conclusions

Ultrathin single and 4Q silicon diodes of interest for beam position and monitoring in synchrotron and particle therapy medical applications are studied. Devices with silicon thicknesses of 10 μm, 5 μm and 3 μm have been successfully fabricated from SOI substrates. Physical and electrical characterization of the devices have been carried out, obtaining good functional electrical characteristics for the devices on the different silicon thicknesses. The impact of different particle irradiations on device electrical characteristics has been assessed for the 10 μm-thick devices. Whereas radiation-induced leakage current increase and positive charge trapping in interquadrant isolation have been observed, functional operation as radiation detector has been verified upon illumination with a pulsed laser beam transient current technique.

Further studies are required for a better evaluation of the fabricated devices, especially the thinnest ones, which would allow maximum transmission. In particular, to assess device performance as radiation detector and reliability in the intended radiation environments. This will include not only laboratory test with laser beam transient current technique, but also an already granted access to XALOC beamline at ALBA Synchrotron in Cerdanyola del Vallès (Barcelona), as well as other possible test beams in particle therapy beam facilities.

## Declaration of Competing Interest

The authors declare that they have no known competing financial interests or personal relationships that could have appeared to influence the work reported in this paper.

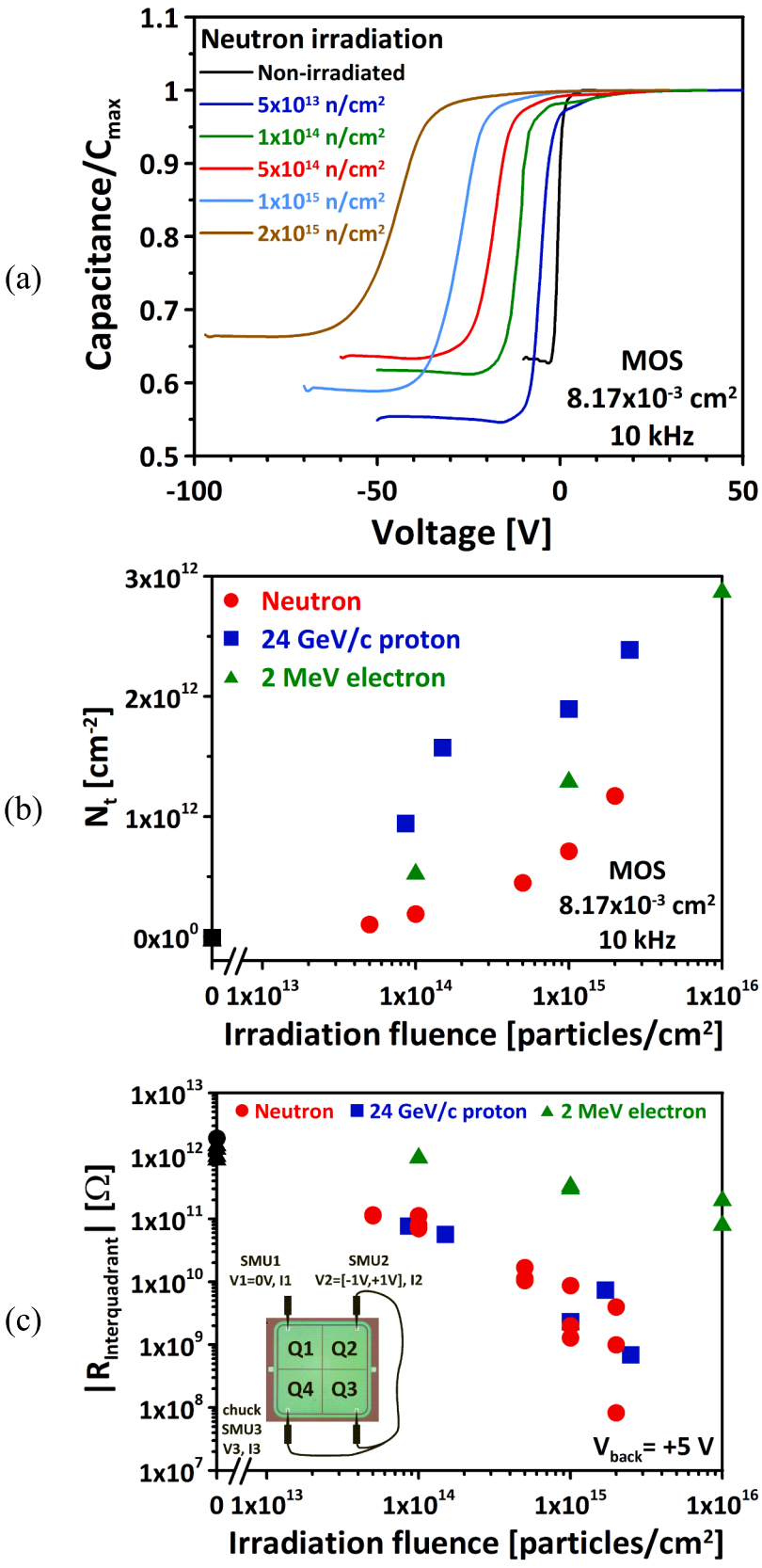


**Fig. 6.** (a) C-V characteristics measured for MOS capacitors using the diode interquadrant $SiO_2$ field oxide irradiated at different neutron fluences. (b) Extracted values for effective trapped charge density ($N_t$) in the dielectric for MOS capacitors at different electron, neutron and proton fluences. (c) Interquadrant resistance measured for 10 μm-thick 4Q diodes at different electron, neutron and proton fluences. The inset shows a sketch of $R_{interquadrant}$ measurement conditions ($R_{interquadrant} = 1/|(dI_1/dV_2)|$) [8].

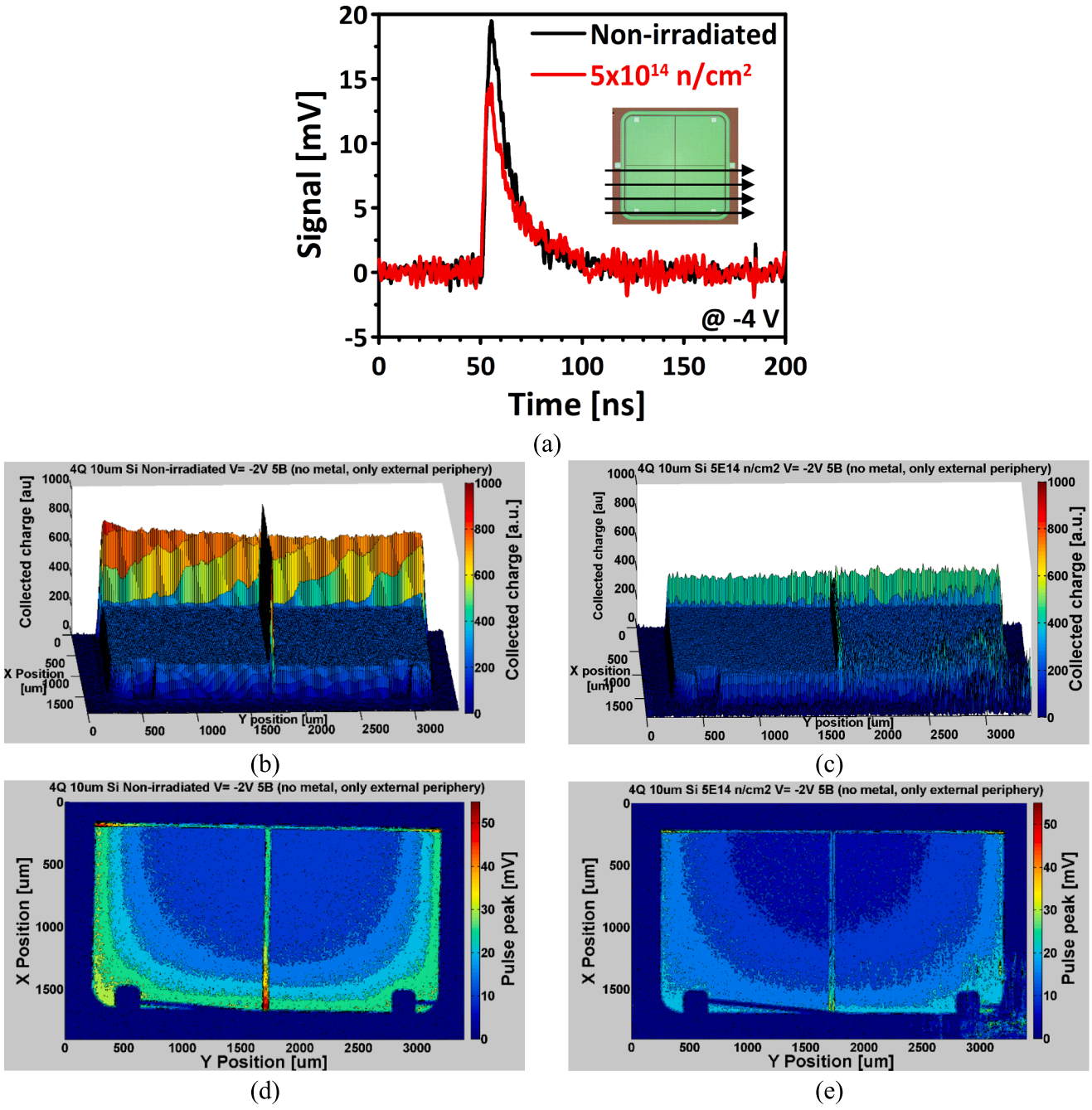


**Fig. 7.** (a) Example of device signal obtained on 10 μm-thick Si non-irradiated and $5 \times 10^{14}$ neutron/cm$^2$ irradiated devices. The inset shows a sketch of the 2 adjacent quadrants scanned with the pulsed laser transient current technique. (b) and (d) 3D plots of collected charge and (c) and (e) 2D contours of transient amplitudes measured for 10 μm-thick Si devices non-irradiated and irradiated at $5 \times 10^{14}$ neutron/cm$^2$.

## Data availability

Data will be made available on request.

## Acknowledgements

This work was supported in part by the Spanish Ministry of Science, Innovation and Universities through the Nuclear and Particle Physics program project PID2021-124660OB-C22 and it has received funding from the EU Horizon 2020 Research and Innovation programme under Grant Agreement no. 654168 (AIDA-2020). It has been partially performed within a collaborative research project at Nuclear Professional School, School of Engineering, The University of Tokyo (Grant # 20016) and it has made use of the Spanish ICTS Network MICRONANOFABS partially supported by MINECO. X. Borrisé is acknowledged for FIB, SEM and EDX inspections. R. Durà and J. Pallarès are acknowledged for reverse engineering inspections. V. D. and T. C. acknowledge the Erasmus+ programme of the European Union.

## References

[1] Fuchs MR, et al. Transmissive x-ray beam position monitors with submicron position- and submillisecond time resolution. Rev Sci Instrum 2008;79:063103. https://doi.org/10.1063/1.2938400.

[2] Durante M, Paganetti H. Nuclear physics in particle therapy: a review. Rep Prog Phys 2016;79(9):096702. https://doi.org/10.1088/0034-4885/79/9/096702.

[3] Cruz C, et al. 10 μm thin transmissive photodiode produced by ALBA Synchrotron and IMB-CNM-CSIC. J Instrum 2015;10:C03005. https://doi.org/10.1088/1748-0221/10/03/C03005.

[4] Morse J, Solar B, Graafsma H. Diamond X-ray beam-position monitoring using signal readout at the synchrotron radiofrequency. J Synchrotron Radiat 2010;17:456–64. https://doi.org/10.1107/S0909049510016547.

[5] Nida S, Tsibizov A, Ziemann T, Woerle J, Moesch A, Schulze-Briese C, et al. Silicon carbide X-ray beam position monitors for synchrotron applications. J Synchrotron Radiat 2019;26(1):28–35. https://doi.org/10.1107/S1600577518014248.

[6] Rafí JM, Pellegrini G, Godignon P, et al. Four-quadrant silicon and silicon carbide photodiodes for beam position monitor applications: electrical characterization and electron irradiation effects. J Instrum 2018;13:C01045. https://doi.org/10.1088/1748-0221/13/01/C01045.

[7] Rafi JM, Pellegrini G, Godignon P, Ugobono SO, Rius G, Tsunoda I, et al. Electron, neutron and proton irradiation effects on SiC radiation detectors. IEEE Trans Nucl Sci 2020;67(12):2481–9. https://doi.org/10.1109/TNS.2020.3029730.

[8] Rafí JM, Pellegrini G, Quirion D, Hidalgo S, Godignon P, Matilla O, et al. 10 μm-thick four-quadrant transmissive silicon photodiodes for beam position monitor application: electrical characterization and gamma irradiation effects. J Instrum 2017;12(01):C01004. https://doi.org/10.1088/1748-0221/12/01/C01004.

[9] Andricek L, et al. Processing of ultra-thin silicon sensors for future e+e- linear collider experiments. IEEE Trans Nucl Sci 2004;51(3):1117–20. https://doi.org/10.1109/TNS.2004.829531.

[10] Kramberger G, Advanced transient current technique systems, *Proc Sci* (Vertex 2014), 2015;032, https://doi.org/10.22323/1.227.0032.